International Journal of Scientific Research in Science, Engineering and Technology

Print ISSN - 2395-1990
Online ISSN : 2394-4099

OPEN ACCESS

Available Online at : www.ijsrset.com
doi : https://doi.org/10.32628/IJSRSET23103211

Numerical Solution of Inviscid and Viscous Flow Across NACA0010 Airfoil with different Angles of Attack

Mohammad Erfan Khodabakhshi*[1], Masoud Aryanpour[2]

*[1] Department of Mechanical Engineering, Sharif University of Technology, Tehran, Iran

[2] Department of Mechanical Engineering, Sharif University of Technology, Tehran, Iran

ARTICLEINFO

Article History :

Accepted: 01 Aug 2023
Published: 18 Aug 2023

Publication Issue :
Volume 10, Issue 4
July-August-2023

Page Number :
268-279

ABSTRACT

The role of the airfoil in all engineering fields is very important. Airfoil designs are utilized in various applications such as aircraft wings, helicopter rotor blades, sails, fans, and turbine compressors. In the case of aircraft, airfoils are accountable for generating lift force and determining if it is adequate for balancing the aircraft's weight, as well as determining the amount of drag force that should be applied to the body. They also play a vital role in optimizing blade performance, as well as the heat and operational efficiency of turbines. Airfoils are moving in the flow passing by them, and they show different responses based on many parameters such as whether the flow is smooth or turbulent, viscous or inviscid, flow velocity, angle of attack, multidimensionality of velocity components, etc. For aeronautics vehicles and wind turbines, a large number of studies have been conducted to analyze aerodynamic forces on two dimensional airfoils as well as flow phenomena associated with different Reynolds numbers. Main object of this research is to figure out the flow characteristics around the airfoil body and analyze aerodynamic performance of airfoil. In order to investigate the computational efficiency of flow models, numerical examination has been done for flow across NACA0010 airfoil by using 2D Computational Fluid Dynamics (CFD) solver, ANSYS FLUENT 18.0, at various angle of attack (0^o to 13^o) for inviscid flow and (-30^o to 30^o) for viscous flow. Lift and drag coefficients and C_p for lower and upper airfoil surface and velocity diagram based on different angle of attack has been solved for the sample under two different flow regimes. The contours of velocity were simulated, and stall point was noticed from 13° angle of attack in inviscid flow and 24^o in viscous flow. In the non-viscous state, lift coefficient and drag coefficient was higher, in comparison with viscous flow.

Keywords: Airfoil, viscous flow, inviscid flow, NACA0010, ANSYS FLUENT, angle of attack

I. INTRODUCTION

Airfoils can be found in sizes ranging from the wings of unmanned aerial vehicles to the blades of wind turbines to the wings of large commercial aircraft and are essential for many engineering applications [1]. In addition, airfoils are capable of operating at a range of speeds, from slow to supersonic speeds [2]. Wind turbines are widely used devices that capture the energy of the wind to generate electricity. Small wind turbines are commonly used on residential rooftops, farms, isolated communities, and boats [3].

The technical challenge for engineers as regards the intended performance of an airfoil lies in such broad areas of application, which use airfoils. Consequently, multiple airfoil configurations have been examined at a diverse array of operating circumstances, such as the Reynolds number, to achieve various aerodynamic efficiencies [4, 5].

The complexity of the simulation and analysis increases as additional physical phenomena are taken into account (e.g., if turbulent, compressible, and multiphase flows are considered, along with other pertinent conditions) [6].

Many experimental investigations and numerical simulations have been conducted to assess the aerodynamic coefficients.

Kamada et al. conducted an investigation on the impact of turbulence on the dynamic stall characteristics of the Horizontal Axis Wind Turbine (HAWT) through wind tunnel experiments. The turbulence flow was generated using turbulence grids. They analyzed the pressure distribution on the blade surface, lift coefficient, and drag coefficient at different angles of attack, considering various turbulence intensities. For an angle of attack of $\alpha = 13°$, the findings revealed that as the angle of attack increased, the lift coefficients in the dynamic state exhibited a greater increase compared to those in the static state. The results also indicated that during dynamic stall, for a Reynolds number (Re) of 1.5×10^5, the flow separated at the leading edge of $x/c > 0.1$ as the angle of attack increased. For a Re of 2.0×10^5, the range of the pressure hysteresis loop became narrower compared to that observed at a turbulence intensity of $Re = 1.5 \times 10^5$ [7].

In the study conducted by Gerakopolous et al., the researchers examined the lift and separation bubble properties of a NACA0018 airfoil through experimental methods. They presented surface pressure measurements for various Reynolds numbers ranging from 80×10^3 to 200×10^3 and angles of attack spanning from 0° to 18°. These measurements were utilized to understand the characteristics of the separation bubble and determine the lift coefficients. Based on the findings, two distinct regions were identified in the lift curves: one with a rapid and linear increase in lift coefficients at low angles of attack, and another with a more gradual and linear growth at higher pre-stall angles. The slope of the lift curve in each region was found to be correlated to the rates of change in separation, transition, and reattachment locations as the angle of attack varied [8].

Aono and Anyoji's study examines the airfoil dynamics at low Reynolds numbers (10^4). They created an airfoil design for the cross-sectional shape of a main wing on a fixed-wing aircraft on Mars. They conducted numerical simulations in both two and three dimensions, as well as experimental measurements of force and flow, to comprehend how the aerodynamic coefficients relate to the flow structures around the airfoil. Findings indicated that the suggested airfoil displayed superior aerodynamic performance compared to the SD7003 airfoil and Ishii airfoil at a Reynolds number of 20,000 [9].

Shahin examined the lift and drag characteristics of the NACA0015 airfoil through a combination of numerical and practical analysis. The airfoil was tested at various attack angles and low Reynolds numbers (Re), with force measurements taken every two degrees from 0° to 20°. The practical experiment was conducted in a low-speed wind tunnel, while the numerical analysis utilized the FLUENT CFD program. The findings from both the experiment and numerical analysis were compared. The stall angle, which is influenced by

turbulence occurring behind the airfoil, was determined. Furthermore, the impact of the stall angle on the airfoil's performance was investigated as a result of the study [10].

Previous studies have demonstrated that both the incident angles and the Reynolds number significantly impact the aerodynamic efficiency of 2D airfoils.

A flow is considered inviscid when the viscosity is extremely low or negligible, meaning there is no friction between the layers of the fluid. Furthermore, there is minimal diffusion of mass and conduction of heat between the particles. Because Reynolds is inversely proportional to the viscosity, which is approaching zero, the Reynolds number is approaching infinity in inviscid flow. On the other hand, it is known as a viscous flow if there are viscosity forces present. Between the layers of the fluid, friction forces are acting. For viscosity flows, the Reynolds number is not infinite. In practical terms, regardless of the magnitude of the force, all flows are essentially viscous, as there is always some degree of viscosity in all flows, [11].

In viscous flow, the speed at the surface of the object will be zero. Because of the existence of the viscosity, there will be a disparity in the pressure distribution and also the shear stress will change along the object. As a result, the overall imbalanced forces will not be zero and the object will generate aerodynamic forces like lift and drag. The pressure surrounding the surface of the object will not be evenly spread out since speed will vary along the flow lines. Particle diffusion and heat conduction will take place among the particles [11].

The fluid dynamics around airfoils can be observed using advanced optical devices. Particle image velocimetry (PIV) is a commonly used optical technique for quickly mapping flow patterns. The fluid is infused with particles that are illuminated and their positions visually documented [12].

Main objects of this research are:

- Drawing C_L, C_D and C_L/C_D graphs according to changes in angle of attack for inviscid and viscous flow regime
- Drawing the graphs of the pressure coefficient for the upper and lower surfaces of the airfoil at each angle of attack for inviscid and viscous flow regime
- Drawing the velocity diagram and stream lines on airfoil surfaces for inviscid and viscous flow regime for angles of attack 0,5,10,15

II. METHODS AND MATERIAL

II-A. Airfoil Force Analysis

As shown in Figure 1, according to Benson's research, when the airfoil is moved across airflow it generates an aerodynamics force on its surface [13].

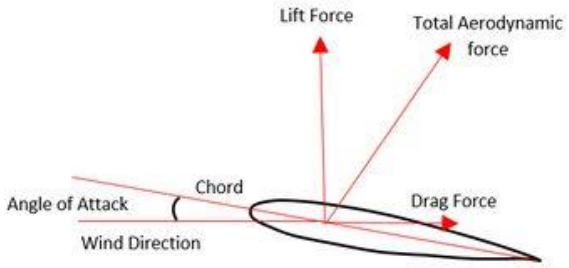

Figure 1: Forces on Airfoil

Because of the configuration of the Airfoil, a disparity in pressure is formed between the upper and lower surfaces of the airfoil. This occurs because the air moves at a higher speed on the upper surface in comparison to the lower surface. As a result, according to Bernoulli's principle [14], a region of low pressure is formed on the upper surface.

The angle of attack is the angle created by the wind direction and the chord, as depicted in Figure 1. The angle of attack rises as the airfoil's leading edge, or the front point, ascends, resulting in a rise in both lift and drag force [15].

The density of fluid and relative velocity between an object and a fluid are, as shown in the equation 1 and 2, respectively proportional to lift and drag forces on any object [16]:

$$C_L = \frac{L}{\frac{1}{2}\rho V_\infty{}^2 A} \quad (1)$$

$$C_D = \frac{D}{\frac{1}{2}\rho V_\infty{}^2 A} \quad (2)$$

Commercial computational fluid dynamics (CFD) software is utilized to conduct numerical investigations. In order to accurately identify changes in flow with individual parameters, computation fluid dynamics consists of a variety of turbulence models.

The choice of airfoils should be determined by a set of requirements. ANSYS is one of the most frequently utilized software in this field, and it is employed to acquire precise outcomes while simulating airfoils.

This study aims to look at an airfoil NACA0010 with various airflow angles using ANSYS and 2D CFD (Computational Fluid Dynamics) simulation.

The NACA0010 wing section is identical; the 00 suggests that it lacks chamber. The 10 suggests that the wing section has a 10% proportion of thickness to chord length; it is 10% as thick as its length.

Using a CFD solver, at various angles of attack for both types of flow, the pressure distribution, lift and drag coefficients will be estimated on each airfoil profile and stalling points. NACA airfoils geometries were obtained as coordinate vertices, i.e., written documents, and imported into the ANSYS programming.

II-B. Simulation

The airfoil profile, boundary conditions, and meshes were all created in the Workbench. To start the simulation, the airfoil geometry was defined. Airfoil geometry was received from "Airfooltool" website and imported to ANSYS CFD and a planar surface from the geometry we defined [17]. Table I shows the data that was used from the Airfooltool Database and imported into the ANSYS workbench with Notepad.

Origin of the coordinates has been defined on the end of the airfoil fin. The drawn airfoil has a chord length and thickness of 1m and 0.1 m respectively. Figure 2 shows the image of the airfoil geometry drawn in CFD. To simulate flow around the airfoil, the airfoil was sketched in a C-shape domain with a size of 12.5m for both the semicircle and the rectangle which is represented in Figure 3.

TABLE I

NACA 0010 AIRFOIL POINTS COORDINATES

NACA 0010			
#Point	X-Cord	Y-Cord	Z-Cord
1	0.000000	0.000000	0.000000
2	0.012500	0.015780	0.000000
3	0.025000	0.021780	0.000000
4	0.050000	0.029620	0.000000
5	0.075000	0.035000	0.000000
6	0.100000	0.039020	0.000000
7	0.150000	0.044550	0.000000
8	0.200000	0.047820	0.000000
9	0.250000	0.049520	0.000000
10	0.300000	0.050020	0.000000
11	0.400000	0.048370	0.000000
12	0.500000	0.044120	0.000000
13	0.600000	0.038030	0.000000
14	0.700000	0.030530	0.000000
15	0.800000	0.021870	0.000000
16	0.900000	0.012070	0.000000
17	0.950000	0.006720	0.000000
18	1.000000	0.001050	0.000000
19	0.950000	-0.006720	0.000000
20	0.900000	-0.012070	0.000000
21	0.800000	-0.021870	0.000000
22	0.700000	-0.030530	0.000000
23	0.600000	-0.038030	0.000000
24	0.500000	-0.044120	0.000000
25	0.400000	-0.048370	0.000000
26	0.300000	-0.050020	0.000000
27	0.250000	-0.049520	0.000000
28	0.200000	-0.047820	0.000000
29	0.150000	-0.044550	0.000000
30	0.100000	-0.039020	0.000000
31	0.075000	-0.035000	0.000000
32	0.050000	-0.029620	0.000000
33	0.025000	-0.021780	0.000000
34	0.012500	-0.015780	0.000000
35	0.000000	0.000000	0.000000

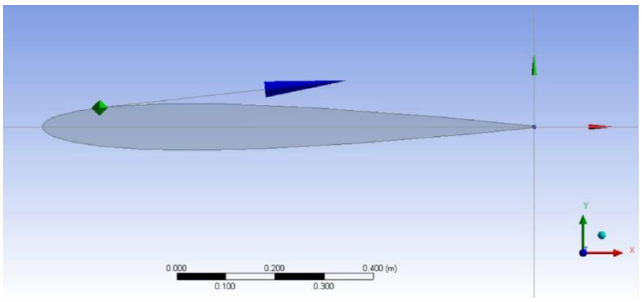

Figure 2: Airfoil Geometry in ANSYS

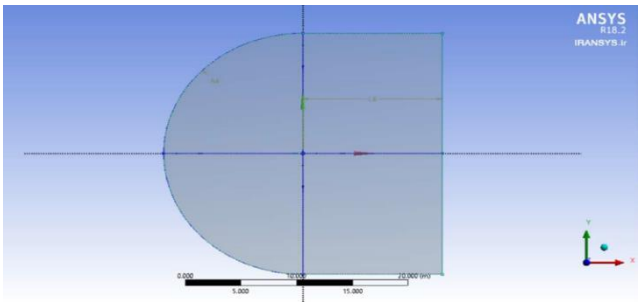

Figure 3: Flow area around Airfoil

The decision to use C-type topology in the simulation was made due to the benefits offered by the structured quadrilateral element, which included increased control and precision, reduced memory usage, and faster convergence.

The precision of the grid was more impressive, near the airfoil boundary layer regions where higher computational precision was required. A mesh refinement has been done for simulation to transform the unsuitable meshing to appropriate mesh. Flow area had been divided into 3 areas and cells have been located in the way that the meshes are smaller in the areas where there are changes in geometry and tension, and the meshes are coarser in the rest of the areas. Figure 4 shows flow area before refinement, while Figure 5 represents meshed flow area after modification.

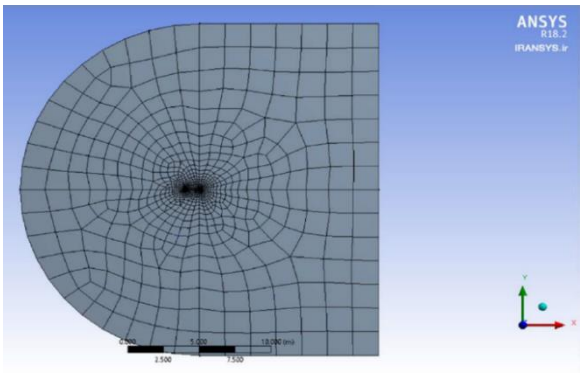

Figure 4: Flow area mesh before refinement

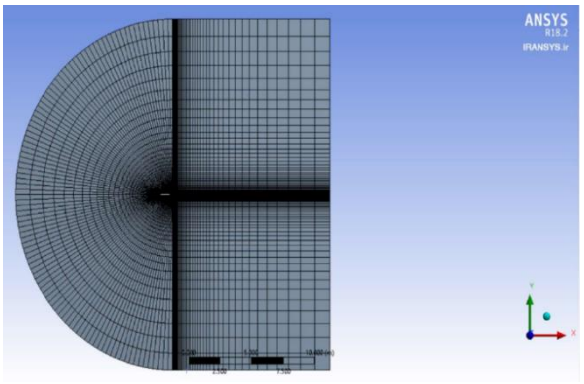

Figure 5: Flow area mesh after refinement

In the boundary conditions section, airfoil geometry was defined as a wall. No slip wall boundary condition is set on the airfoil surface. "Pressure outlet" was selected and gauge pressure set to zero. The nose of the airfoil was defined as the source of pressure and the gauge pressure set to 101325 Pa.

In the flow simulation, magnitude and direction method was used to apply the fluid velocity. X component of fluid velocity set absolutely at 1m/s and simulation was applied for steady time state. Y component of velocity was set based on angles of attack ($V_y = V_x * \tan(AoA)$) and the angles of attack were set to degrees from 0 to where stall happened for inviscid flow simulation and -30° to 30° for viscous flow. Simulation reference for the calculation of physical values has been set as inlet. As the fluid is air, mechanical properties of air have been applied for simulation. Temperature set at 288.16 kelvin and

density set at 1.225 kg/m3. Second-order upwind model is applied for discretization of convection term due to its accuracy in calculation [18].

III.RESULTS AND DISCUSSION

III-A. Inviscid flow Results

After solving the problem, the fluid velocity contour, the C_p coefficient on the upper and lower surfaces of the airfoil, the drag and lift coefficient were obtained. By changing the angle of attack and keeping other parameters constant, C_p and C_L values were obtained for all angles of attack. C_p coefficient on the upper and lower surfaces of the airfoil diagram for angles 0, 1, 3, 5, 8, 10, 13 degree as shown in Figures 6-12.

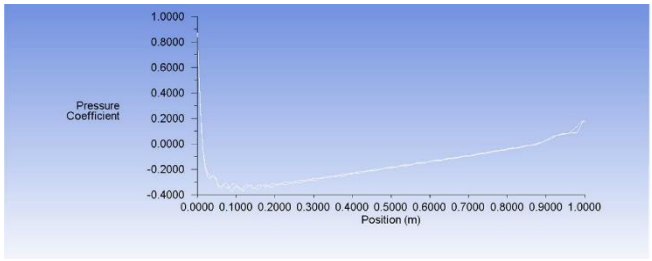

Figure 6: C_p coefficient on the upper and lower surfaces of the airfoil under inviscid flow for Angle of Attack 0 degree

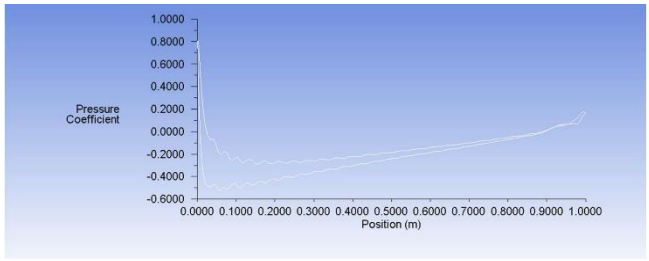

Figure 7: C_p coefficient on the upper and lower surfaces of the airfoil under inviscid flow for Angle of Attack 1 degree

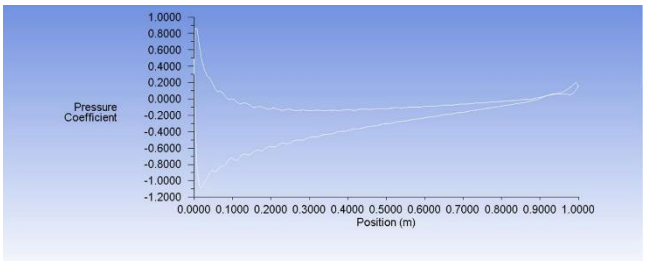

Figure 8: C_p coefficient on the upper and lower surfaces of the airfoil under inviscid flow for Angle of Attack 3 degree

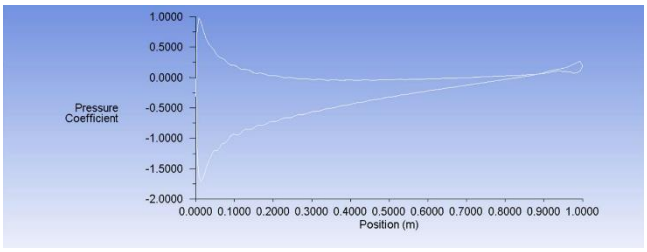

Figure 9: C_p coefficient on the upper and lower surfaces of the airfoil under inviscid flow for Angle of Attack 5 degree

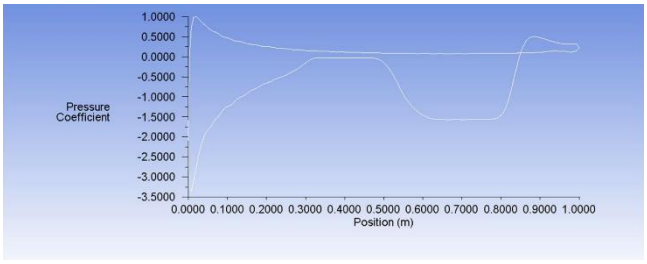

Figure 10: C_p coefficient on the upper and lower surfaces of the airfoil under inviscid flow for Angle of Attack 8 degree

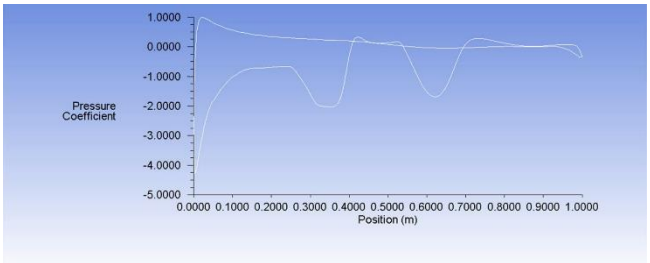

Figure 11: C_p coefficient on the upper and lower surfaces of the airfoil under inviscid flow for Angle of Attack 10 degree

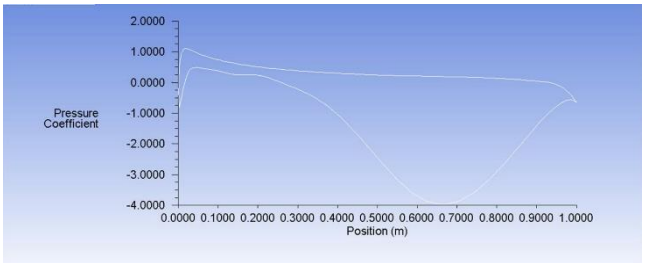

Figure 12: C_p coefficient on the upper and lower surfaces of the airfoil under inviscid flow for Angle of Attack 13 degree

In the next step, using calculated C_p diagram, drag and lift coefficients has been resulted. Figure 13 and Figure 14 represent angle of attack chart in terms of C_L and C_D coefficient, respectively.

As it is clear in the Lift coefficient diagram, the stall phenomenon occurred at the angle of attack of 13 degrees.

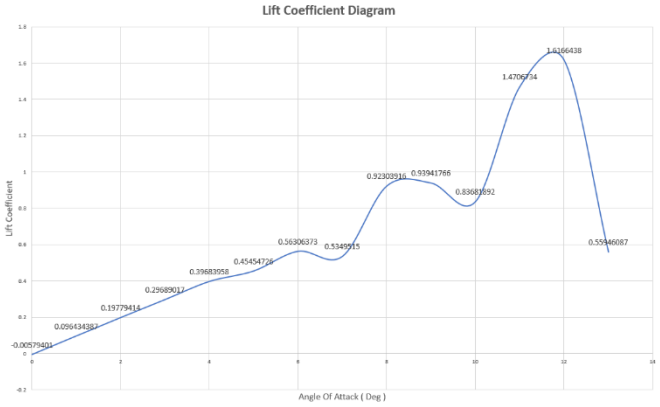

Figure 13: Lift coefficient for inviscid flow by different attack angles diagram

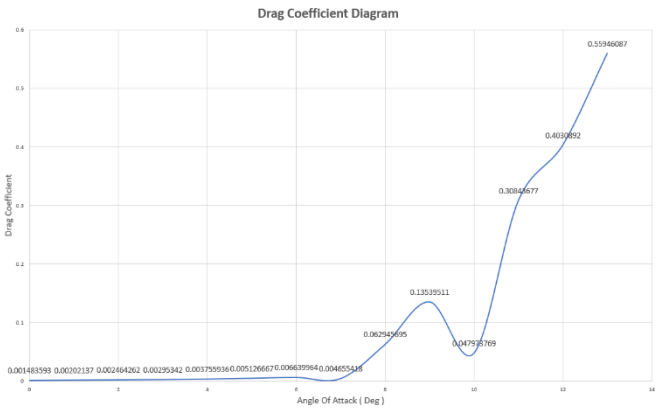

Figure 14: Drag coefficient for inviscid flow by different attack angles diagram

To enhance the power coefficient and the generated torque, it is essential to optimize the lift coefficient, C_D, and the lift to drag ratio (L/D ratio) of the airfoil [19, 20]. The L/D ratio plays a significant role in evaluating the performance of the airfoil. When L/D ratio is high it shows the drag coefficient has very less value. The L/D ratio for NACA 0010 is shown in Figure 15.

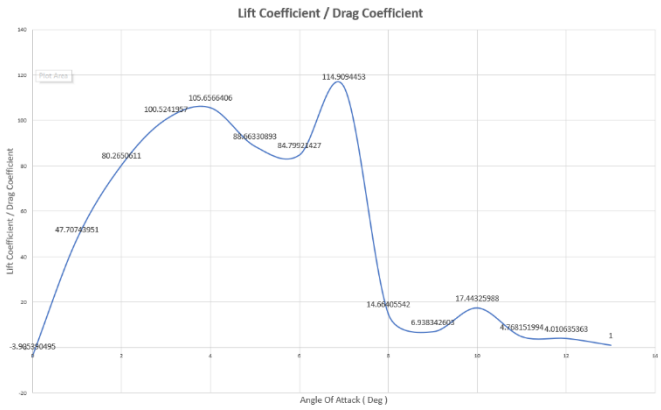

Figure 15: C_L/C_D ratio for inviscid flow by different attack angles diagram

Figures 16, 17, 18 shows velocity contours of airfoil for 0, 5, 10 degrees. As it can be seen, when the angle of attack increases positively from zero angle, the stagnation point is moved toward the trailing edge on the bottom surface. Thus, the lift coefficient will continue increase with angle of attack until maximum in stall angle then start to decrease.

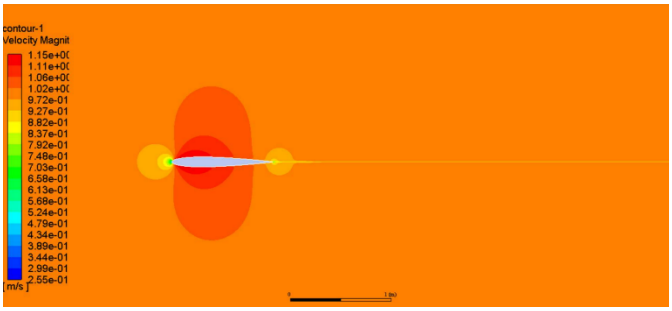

Figure 16: Velocity contour of airfoil under inviscid flow when AoA is 0 degree

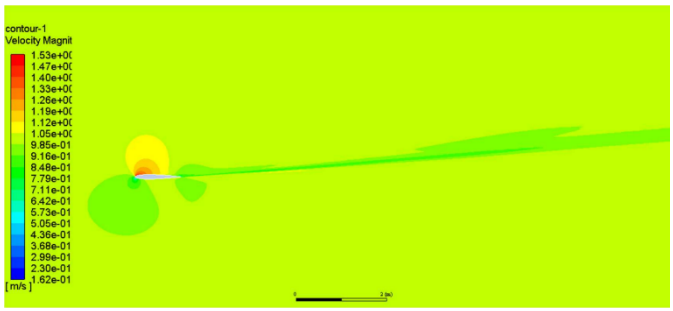

Figure 17: Velocity contour of airfoil under inviscid flow when AoA is 5 degree

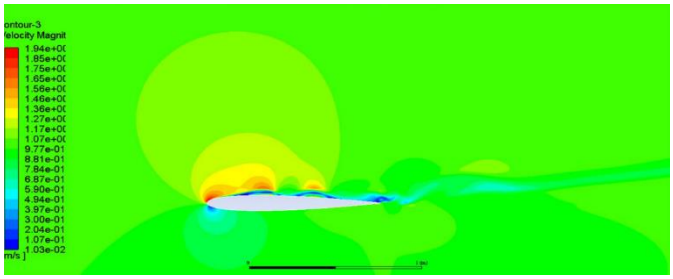

Figure 18: Velocity contour of airfoil under inviscid flow when AoA is 10 degree

III-B. Viscous flow Results

In order to simulate the viscous flow, the Reynolds number is considered to be 1000000, and according to the inlet velocity of 1 meter per second and the airfoil length of 1 meter, the viscosity of the fluid is 1.225e-6. In the following, we do not network the problem in order to reach an independent network. After we reached the independent network, we changed the attack angles of the flow so that the C_L and C_D diagrams are the same according to different angles. A graph of lift coefficient versus angle of attack was plotted as shown as Figure 19 while a graph of drag coefficient versus angle of attack was plotted as shown as Figure 20. By observing the graph in Figure 19 can be noticed that the lift coefficient increases linearly while increasing the angle of attack at low angle of attack which is in the range of -16° to 24°. At increased angle of attack, the upper surface airflow of the airfoil initiated detachment. The airflow no longer adheres to the airfoil's surface. This occurs in a section above the upper surface and close to the airfoil's trailing edge. In this area, the speed is diminished and the airflow undergoes a turbulent reversal. This separated airflow is referred to as trailing edge separation [21].

As the angle of incidence is increased further, the detachment flow area continuously shifts towards the front edge. At a specific critical angle of incidence, the lift factor will plummet swiftly and drag factor will escalate swiftly. This circumstance was dubbed stall and the angle of incidence where the stall commences was recognized as the stall angle. In the stall angle, the airfoil will have a maximum lift coefficient [22]. As it can be seen, the stall phenomenon occurred for attack angles greater than 24°.

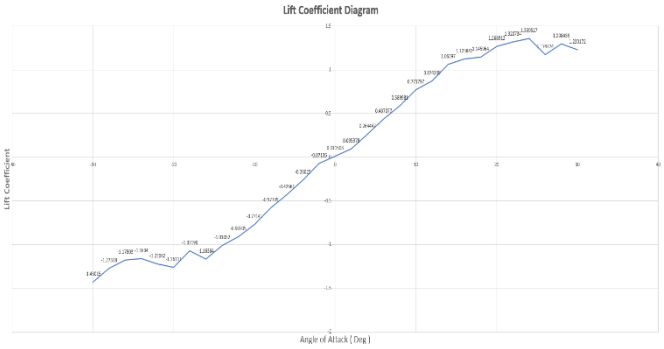

Figure 19: Lift coefficient for viscous flow by different attack angles diagram

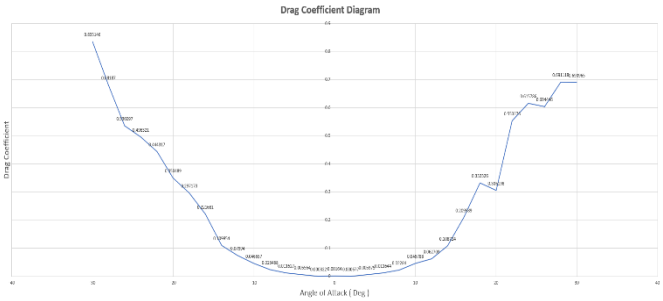

Figure 20: Drag coefficient for viscous flow by different attack angles diagram

Ratio of C_L/C_D is represented in Figure 21.

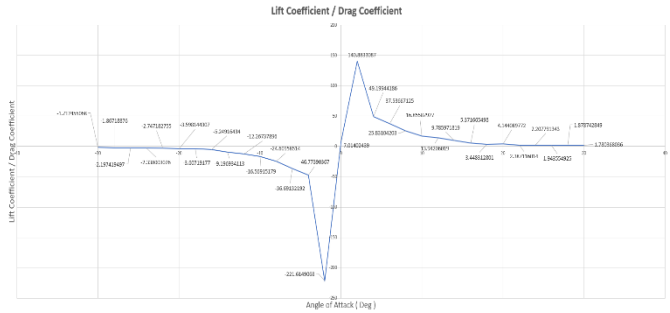

Figure 21: C_L/C_D ratio for viscous flow by different attack angles diagram

The distribution of pressure coefficient on NACA 0010 airfoil at different angle of attack in different turbulence models are shown as Figures 22-25.

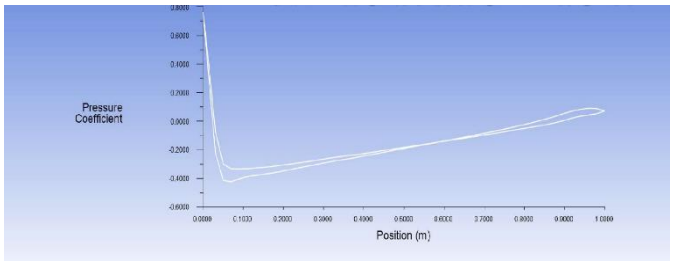

Figure 22: C_p coefficient on the upper and lower surfaces of the airfoil under viscous flow for Angle of Attack 0 degree

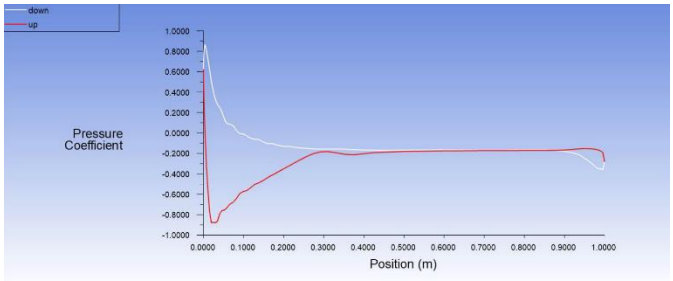

Figure 23: C_p coefficient on the upper and lower surfaces of the airfoil under viscous flow for Angle of Attack 5 degree

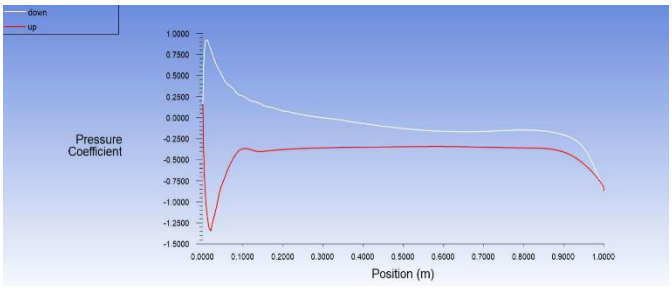

Figure 24: C_p coefficient on the upper and lower surfaces of the airfoil under viscous flow for Angle of Attack 10 degree

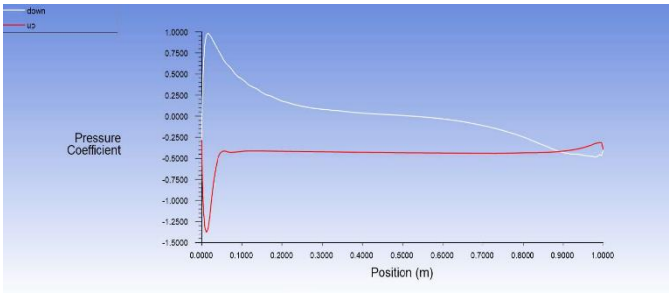

Figure 25: C_p coefficient on the upper and lower surfaces of the airfoil under viscous flow for Angle of Attack 15 degree

It can be seen that pressure coefficient of upper was negative and lower surface was positive when the angle is more than zero.

Figures 26-31 shows stream lines and velocity contours of airfoil for 5, 10, 15 degrees. As it can be seen, when the angle of attack increases positively from zero angle, the stagnation point is moved toward the trailing edge on the bottom surface. Thus, the lift coefficient will continue increase with angle of attack until maximum in stall angle then start to decrease.

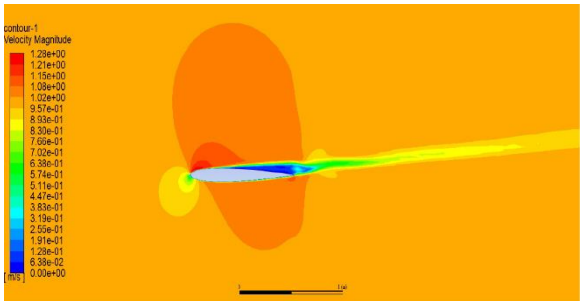

Figure 26: Velocity contour of airfoil under viscous flow when AoA is 5 degree

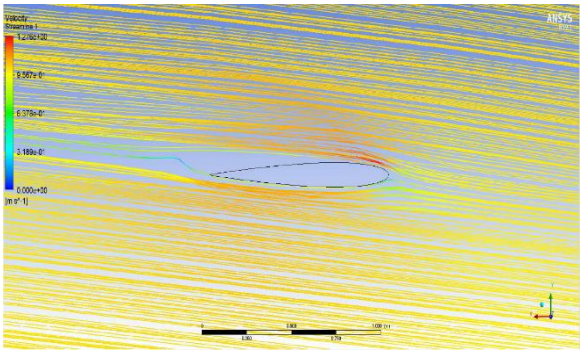

Figure 27: Streamline contour of airfoil under viscous flow when AoA is 5 degree

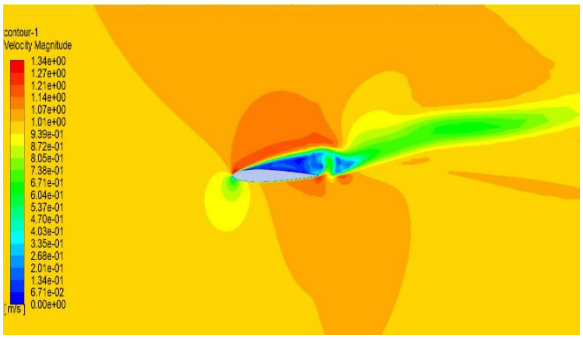

Figure 28: Velocity contour of airfoil under viscous flow when AoA is 10 degree

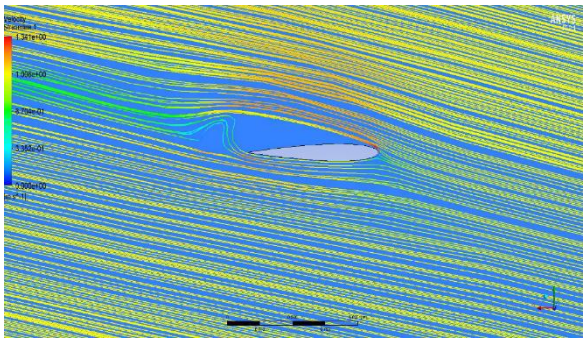

Figure 29: Streamline contour of airfoil under viscous flow when AoA is 10 degree

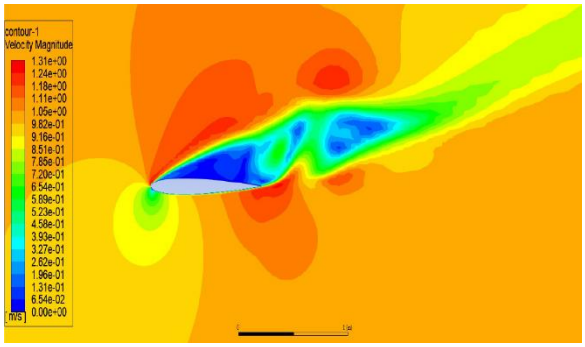

Figure 30: Velocity contour of airfoil under viscous flow when AoA is 15 degree

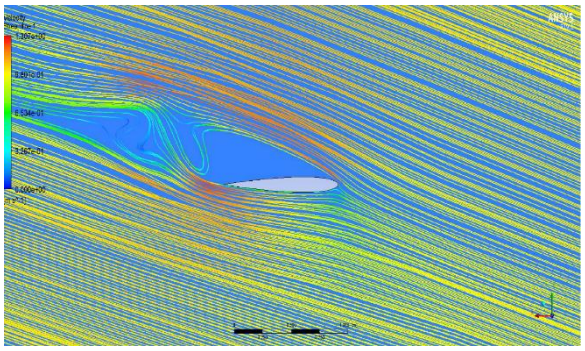

Figure 31: Streamline contour of airfoil under viscous flow when AoA is 15 degree

IV.CONCLUSION

ANSYS Workbench fluent software Simulation was utilized to choose and analyze airfoil NACA0010. The objective of this investigation is to determine the effectiveness of the airfoil by conducting a range of calculations at different angles of attack for both non-viscous and viscous flows. Upon comparing the outcomes for various angles of attack, it is evident that NACA0010 experiences stall at an angle of 13 degrees in non-viscous flow and 24 degrees in viscous flow.

The angle of attack was increased to achieve the ideal lift coefficient. Based on the data provided in the Figure 13, as the angle of attack rises, the lift coefficient also increases, until the angle of attack reaches 13°, at which stage the lift coefficient starts to decline, and the angle of attack 13 is identified as the point of stall,

where the airfoil's highest lift coefficient is observed. It can be observed from Figure 15 and Figure 21 that the airfoil's highest effectiveness is attained at an angle of attack 7^o and 2^o in inviscid and viscous flow regime, respectively.

As the angle of attack increases beyond the point of stalling, the separation of air will also become apparent. Furthermore, a vortex develops as the angle of attack increases, as shown in Figures 26-31.

Using Table II, C_D and C_L coefficients for viscous and non-viscous flows for different angles of attack can be compared. As it is clear from the table, in the non-viscous state, the lift and drag coefficient is higher.

TABLE III

C_L AND C_D COMPARISON BASED ON DIFFERENT AOA

Angle of Attack	C_L		C_D	
***	Viscous	Inviscid	Viscous	Inviscid
0	0.01150	-0.00579	0.00164	0.00148
5	0.35076	0.45455	0.00851	0.00513
8	0.58998	0.92304	0.02284	0.06295
10	0.77180	0.83682	0.04579	0.04797
12	0.87421	1.61665	0.06270	0.40309

V. REFERENCES

[1] SRL. Samion and MSM. Ali. "Aerodynamic noise measurement in anechoic wind tunnel of rod-airfoil with leading edge serrations," Journal of Advanced Research in Fluid Mechanics and Thermal Sciences, vol.47, 2018, pp. 97-107.

[2] P. Rojratsirikul, Z. Wang, I. Gursul. “Unsteady fluid–structure interactions of membrane airfoils at low Reynolds numbers," Animal Locomotion, 2010, pp. 297-310.

[3] O. Ozgener, L. Ozgener. "Exergy and reliability analysis of wind turbine systems: a case study." Renewable and Sustainable Energy Reviews, vol.11, 2007, pp. 1811-1826.

[4] J. Winslow, H. Otsuka, B. Govindarajan, I. Chopra. "Basic understanding of airfoil characteristics at low Reynolds numbers (104–105)." Journal of aircraft, vol.55, 2018, pp. 1050-1061.

[5] X. Shen, E. Avital, G. Paul, MA. Rezaienia, P. Wen, T. Korakianitis. "Experimental study of surface curvature effects on aerodynamic performance of a low Reynolds number airfoil for use in small wind turbines." Journal of Renewable and Sustainable Energy, vol.8, 2016, pp. 1-14.

[6] SA. Khan, et al. "Comparing the effect of different turbulence models on the CFD predictions of NACA0018 airfoil aerodynamics." CFD Letters, vol. 12, Issue. 3, 2020, pp. 1-10.

[7] Y. Kamada, T. Maeda, J. Murata, Y. Nishida. "Effect of turbulent inflows on airfoil performance for a Horizontal Axis Wind Turbine at low Reynolds numbers (Part II: Dynamic pressure measurement)." Energy, vol. 112, 2016, pp. 574-587.

[8] R. Gerakopulos, M. Boutilier, S. Yarusevych. "Aerodynamic characterization of a NACA 0018 airfoil at low Reynolds numbers." 40th Fluid dynamics conference and Exhibit, 2010, p. 4629.

[9] H. Aono, M. Anyoji, D. Hamada, S. Wakui, T. Tatsuwaka. "A study on development of airfoil shape toward low reynolds-number dependence of aerodynamic characteristics under low-reynolds-number-flow conditions." AIAA Aerospace Sciences Meeting, 2018, p. 1085.

[10] I. Şahin, A. Acir. "Numerical and experimental investigations of lift and drag performances of NACA 0015 wind turbine airfoil." International Journal of Materials, Mechanics and Manufacturing, vol.3, 2015, pp. 22-25.

[11] https://garudauniverse.com/viscous-vs-inviscid-flow.

[12] F. Wang, L. Bai, J. Fletcher, J. Whiteford, D. Cullen. "The methodology for aerodynamic study on a small domestic wind turbine with scoop." Journal of wind engineering and industrial aerodynamics, vol. 96, 2008, pp. 1-24.
[13] http://en.wikipedia.org/wiki/Lift_coefficient.
[14] MP. Singh, DMS. Khidiya, S. Soni. "CFD Simulation of an Airfoil at different Angle of Attack." International Journal of Scientific Research in Science, vol. 2, Issue. 3, 2016, pp. 773-776.
[15] M. Shinde, V. Shinde, S. Shirode, D. Shriwas. "Simulation of flow over airfoil." Int Res J Eng Technol, 2021, pp. 11-17.
[16] RK. Singh, MR. Ahmed, MA. Zullah, YH. Lee. "Design of a low Reynolds number airfoil for small horizontal axis wind turbines, "Renewable energy, vol.42, 2012, pp. 66-76.
[17] http://airfoiltools.com/airfoil/details?airfoil=naca0010-il.
[18] WY. Tey, RYW. Hong, Y. Asako, HS. Kang, KC. Ng. "Analysis on computational efficiency of convection discretization schemes in SIMPLE algorithm," Journal of Advanced Research in Fluid Mechanics and Thermal Sciences, vol. 58, 2019, pp. 100-117.
[19] R. Lanzafame, M. Messina. "Design and performance of a double-pitch wind turbine with non-twisted blades, " Renewable Energy, vol. 34, 2009, pp. 1413-1420.
[20] MS.Selig, JJ. Guglielmo. "High-lift low Reynolds number airfoil design." Journal of aircraft, vol.34, 1997, pp. 72-79.
[21] J. Yao, W. Yuan, J. Wang, J. Xie, H. Zhou, M. Peng, Y. Sun. "Numerical simulation of aerodynamic performance for two dimensional wind turbine airfoils," Procedia Engineering, vol. 31, 2012, pp. 80-86.
[22] J. Johansen, JN. Sørensen. "Prediction of laminar /turbulent transition in airfoil flows," Journal of aircraft, vol. 36, 1999, pp. 731-734.

Cite this article as :

Mohammad Erfan Khodabakhshi, Masoud Aryanpour, "Numerical Solution of Inviscid and Viscous Flow Across NACA0010 Airfoil with different Angles of Attack", International Journal of Scientific Research in Science, Engineering and Technology (IJSRSET), Online ISSN : 2394-4099, Print ISSN : 2395-1990, Volume 10 Issue 4, pp. 268-279, July-August 2023. Available at doi :
https://doi.org/10.32628/IJSRSET23103211
Journal URL : https://ijsrset.com/IJSRSET23103211